**An update on inert anodes for aluminium electrolysis**

**Yasinskiy A. S.**, Assistant Prof., Cand. Eng. Sci., Head of the Laboratory[1], e-mail: ayainskiykrsk@gmail.com

**Sai Krishna Padamata**, PhD Student, Assistant, Junior Researcher[1], e-mail: saikrishnapadamata17@gmail.com

**Polyakov P. V.**, Professor, Dr. Chem. Sci., Leading Researcher[1], e-mail: p.v.polyakov@mail.ru

**Shabanov A. V.**, Cand. Phys.-Math. Sci., Senior Researcher[2], e-mail: alexch_syb@mail.ru

[1]Laboratory of Physics and Chemistry of Metallurgical Processes and Materials, Siberian Federal University, Krasnoyarsk, Russia.

[2]Laboratory of Molecular Spectroscopy, Krasnoyarsk Science Center SB RAS, Krasnoyarsk, Russia.

This update includes the literature related to the inert anodes which were published in the past decade. The metallic anodes are widely regarded as promising candidates to replace the carbon anodes due to its attractive properties like good electrical conductivity, easy to manufacture and high resistance to high thermal shocks. The metals have been tested in pure state and alloy (binary, ternary) form. The oxide scale formed on the anode surface acts as a barrier between the electrolyte and the anode which protects the anode from being dissolved. The layer of molten fluorides is formed between the scale and the metal anode after a certain time of polarization and the oxide scale acts as a bipolar electrode. Metal like Cu is reduced at the internal side of the scale. This paper elaborates the effects of various parameters on the performance of the anode. Cu-based alloys (Cu – Ni–Fe and Cu–Al) have shown promising results and could perform well in low-temperature electrolytes. It has been well established that the Cu content in Cu–Ni–Fe and Cu–Al alloys plays a major role in the metal dissolution as the $CuO/Cu_2O$ scales formed on the outer layer act as a sacrificial one. The corrosion rate of an anode can be reduced by decreasing the operating temperature which is possible by using the $KF–AlF_3$ melts. The use of suspensions can increase the purity of the produced metal by stopping the anode products to come in contact with cathode metal. Many industries including RUSAL and ELYSIS are still conducting a considerable amount of research to develop an inert anode and are expecting to have a carbon-free cell in the nearest future.

**Keywords:** inert anodes, aluminium electrolysis, $CO_2$ emission, metallic anode, cermet anode, ceramic anode, oxygen-evolving electrode, fluoride melt, corrosion, oxidation, low-temperature electrolyte, Hall-Heroult cell.

## 1. Introduction

The development of inert anodes has become of primary importance for aluminium industries because of its environmental and economical benefits [1–2]. Successful adoption of an inert anode to the electrolysis cell can eliminate the emission of greenhouse gases which happens while using consumable carbon anodes. Although, there is an increasing argument that the introduction of inert anodes in aluminium production can only have a little to none environmental benefits [3]. This update is the continuation of [4], although the paper focuses mostly on the metallic inert anodes, which were investigated in the past decade and are not included in [4]. Many reviews on inert anode development were made in [5–9]. The metallic anodes are preferred among the anode materials (cermets, ceramics and metals) as they possess high electrical conductivity, mechanical robustness, easy fabrication, good thermal resistance and ease in electrically connecting to current leads [10].

The metallic anode is protected by an oxide scale which grows once the anode is immersed into the melt. This layer improves the anodes chemical resistance and protects it from the corrosion.

The following reaction is expected with the anode polarization:

$$M_{(s)} + x\mathrm{O}_{(c)}^{2-} = M\mathrm{O}_{x(s)} + 2xe^{-} \quad (1)$$

For reaction (1), the electrode potential ($E$) is often more negative than the oxygen evolution potential. When $E$ is greater than 2.2 V (oxygen evolution potential vs. $Al^{3+}/Al$), the anodic reaction (2) occurs:

$$2\mathrm{O}_{(c)}^{2-} = \mathrm{O}_{2(g)} + 4e^{-} \quad (2)$$

Subindex ($c$) stands for the complex ions.

To protect the metal anode, the oxide layer should self-renovate itself at the time of electrolysis process [11]. The formation rate of the oxide should be equal or higher to the oxides dissolution rate in the electrolyte. So while selecting the anode material, one should consider the solubility and the dissolution rate of the oxide layer in the melts.

In the past decade, most of the studies were conducted on Cu–Ni–Fe, Fe–Ni and Cu–Al alloys in sodium and potassium cryolite melts at different parameters. In this paper, the studies related to the performance of the carbon-free anodes mostly in the form of alloys and superalloys are discussed.

## 2. Mechanisms of anode corrosion and aluminium contamination

Keller et al. [12] discussed the mass-transport model to calculate the aluminium contamination rate according to the equation:

$$\text{reduction rate} = k_c A_c c_{bulk} \quad (3)$$

where $k_c$, $A_c$, and $c_{bulk}$ are the mass-transport coefficient, the cathodic surface area and the impurity cation concentration.

The life of anode will depend on the dissolution rate of anode corrosion products, which depends on its reduction rate at the cathode. The mass-transport coefficient and the solubility of anode corrosion products should be maintained as low as possible to prolong anode life.

Electrochemical features of corrosion mechanism are studied in several publications. Antipov et al. [13] tested pure metals and binary alloys to find the correlation between the nature of anodes and corrosion resistance. Cyclic voltammetry gave considerably helpful information related to the corrosion mechanism. It was found that alloying plays a crucial role in increasing the corrosion resistivity. Using Cu in alloys is highly advantageous due to the high electrical conductivity and low dissolution rate of its oxides.

Outdot et al. [14] studied the oxide layer growth mechanism low potential polarization of iron, cobalt and nickel in cryolitic melt and concluded that the oxidation follows the common scenario: metal dissolution/spinel precipitation/monoxide growth. It is also stressed that metal fluoride is formed between the oxide layer and the metal during longer duration electrolysis at high current densities due to the oxide ion depletion in the infiltrated electrolyte. This phenomenon was studied in [15] and it was found that metal ions are reduced from this metal fluoride layer on the inner side of the oxide layer. An SEM image showing the presence of metallic copper on the inner side of the oxide layer removed from the 90Cu10Al anode after long term polarization is shown in Fig. 1.

The similar bipolar behaviour of the oxide layer was observed by Khramov et al. [16] tested 82Cu–8Al–5Ni–5Fe anode in the $KF–AlF_3–Al_2O_3$ melt.

Suzdaltsev et al. [17] proposed the mechanism of oxygen evolution based on cyclic voltammogrames recorded on Pt electrodes in $KF–NaF–AlF_3$ melt:

$$x\mathrm{Pt} + \mathrm{Al_2O_2F_4^{2-}} + \mathrm{AlF_6^{3-}} = \mathrm{Pt}_x\mathrm{O} + \mathrm{Al_2OF_6^{2-}} + \mathrm{AlF_{4-}} + 2e^- \quad (4)$$

$$x\mathrm{Pt} + \mathrm{Al_2OF_6^{2-}} + \mathrm{AlF_6^{3-}} = \mathrm{Pt}_x\mathrm{O} + 3\mathrm{AlF_4^-} + 2\mathrm{e^-} \quad (5)$$

are followed by

$$2\mathrm{Pt}_x\mathrm{O} = 2x\mathrm{Pt} + \mathrm{O_2} \quad (6)$$

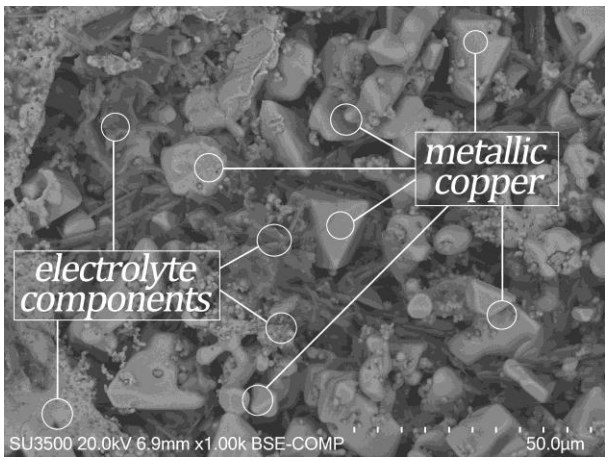


**Fig. 1.** SEM image of the inner side of oxide layer showing the presence of copper rediced from the fluoride layer between the oxide scale and metal (first time presented here)

The other mechanism can be assumed without $Pt_xO$ being formed:

$$2Al_2O_2F_4^{2-} + 2AlF_6^{3-} = O_2 + 2Al_2OF_6^{2-} + 2AlF_4^- + 4e^- \quad (7)$$

$$2Al_2OF_6^{2-} + 2AlF_6^{3-} = O_2 + 6AlF_4^- + 4e^- \quad (8)$$

The process was stated to be quasi-reversible under certain conditions. The same can occur at different quasi-inert anodes at proper potentials. However, significant diffusion limitations were observed in [15] where limiting current densities were as low as 0.3–0.8 A/cm$^2$ in KF – $AlF_3$ melts at 750–850 °C.

The possible application of knowing the oxidation mechanism is using it to synthesize the protective oxide layer with desired properties before the electrolysis (or in-situ) like it was done by Tang et al. [18]. Three layers formed at the 79Ni–10Cu–11Fe anode in $Na_2CO_3$ – $K_2CO_3$ melt were Cu, NiO and $NiFe_2O_4$.

The scale formation and dissolution at Fe–Ni–Cr anodes were studied by Ndong et al. [19]. It is found that the spinel phase is formed at significant overvoltage. A mixture of multiple $M_xO_y$ layers exist on the anode substrate and may have complex microstructure.

Meyer et al. [20] explained the oxidation mechanism of Ni–Fe–O/Cu–Ni–Fe anode. According to the explanation, iron is firstly oxidized into $FeF_2$ in presence of fluorine ion and into FeO with $O^{2-}$ ion. $NiF_2$ and Ni–Fe–O phases are formed from anodic metals. Bath penetration into the anode and leads to the dissolution of fluorides formed. Then $Cu_2O$ is formed by metallic copper oxidation and fully oxidized anodes become non-conductive with only two oxide phases containing Ni being detected. Another study performed by Meyer et al. [21] showed that Iron aluminate had around a twentyfold higher rate of dissolution when compared to the rate of formation. The proposed mechanism of aluminate formation was as follows:

1) substitution between $Fe^{3+}$ located in octahedral site and $Al^{3+}$ from the bath

$Fe^{3+}[Fe^{2+}Fe^{3+}]O_4^{2-} + Al^{3+} = Fe^{3+}[Fe^{2+}Al^{3+}]O_4^{2-} + Fe^{3+}$ (9)

2) site inversion between $Fe^{3+}$ located in thetrahedral site and $Fe^{2+}$ in octahedral site

$Fe^{3+}[Fe^{2+}Al^{3+}]O_4^{2-} = Fe^{2+}[Fe^{3+}Al^{3+}]O_4^{2-}$ (10)

3) substitution between $Fe^{3+}$ located in octahedral site and $Al^{3+}$ from the bath

$Fe^{2+}[Fe^{3+}Al^{3+}]O_4^{2-} + Al^{3+} = Fe^{3+}[Al^{3+}]_2O_4^{2-} + Fe^{3+}$ (11)

$Ni^{2+}$ should be added to the spinel structure to form $NiFe_2O_4$ and prevent rapidly soluble $FeAl_2O_4$ formation.

## 3. Metallic inert anodes

### 3.1. Fe–Ni alloy

Cao et al. [22] studied the electrochemical oxidation behaviour of Fe–Ni alloys with various compositions in 48.2NaF–43.8$AlF_3$–8$Al_2O_3$ molten salts at a working temperature of 980 °C. The findings show that the dissolution potentials (*E*) of Fe–Ni alloys were between 1.11 V (dissolution potential of pure Fe) and 1.33 V (of pure Ni). The *E* increased with an increase in the Ni content of the alloys. The polarization curves of all the Fe–Ni alloys and pure Fe can be distinguished into four regions: active dissolution, active-passive transition, passivation, and transpassivation regions. The current density increased by increasing the applied potential.

When the Fe ions reached a critical concentration at the near-surface region of the electrode, FeO precipitated on the surface of the electrode to form an initial passivation film due to the dissolution–precipitation mechanism. Further, FeO was oxidized to $Fe_2O_3$ at the passivation film–molten salt interface, resulting in the formation of $Fe_2O_3$ as an outer layer. The SEM–EDX examination referred to $Fe_2O_3$ as a main component of the passivation film. Besides, the passivation film formation led the alloy to shift from the non-steady state to a steady state. The passivation film was dismantled during the oxygen evolution due to the lack of alumina. Thereby, the current density raised quickly in the transpassivation region. The preoxidized 43Fe–57Ni alloy showed better resistance toward the corrosion compared to that of the non-oxidated alloy. The chronopotentiometry curve showcases that preoxidized 43Fe–57Ni alloy was very stable during constant-current electrolysis and suggested for further investigated. The anodes with similar compositions were tested in 45KF–50$AlF_3$–5$Al_2O_3$ at 700 °C and similar results were observed, although there was a huge change in the potential and current density at which the passivation of the electrode occurs [23]. The passivation of the anode occurs at low current densities ranging between 0.029–0.079 A/$cm^2$, ten times lower than in sodium cryolite melts. The reason might be the temperature difference. The results are mentioned in Table 1.

**Table 1.**

Details of the passivation region of Fe–Ni anodes in sodium and potassium melts [22–23]

| Composition (wt.%) | $NaF–AlF_3–Al_2O_3$ melt at 980 °C | | | $KF–AlF_3–Al_2O_3$ melt at 700 °C | | |
|---|---|---|---|---|---|---|
| | Passivation potential (V) | Current density at passivation region ($A/cm^2$) | Breakdown Potential (V) | Passivation potential (V) | Passivation Current density ($A/cm^2$) | Breakdown Potential (V) |
| 43Fe–57Ni | 1.61 | 0.55–0.80 | 2.35 | 2.59 | 0.049–0.036 | 2.78 |
| 50Fe–50Ni | 1.53 | 0.49–1.39 | 2.36 | 2.57 | 0.041–0.020 | 2.70 |
| 57Fe–43Ni | 1.49 | 0.56–1.48 | 2.67 | 2.49 | 0.053–0.023 | 2.67 |
| 80Fe–20Ni | 1.64 | 1.36–2.39 | 2.44 | 2.40 | 0.06–0.015 | 2.58 |
| Fe | 1.59 | 1.15–1.49 | 2.24 | 2.43 | 0.079–0.029 | 2.60 |

High-temperature oxidation and corrosion behaviour of 68Fe–32Ni (wt.%) at 970°C in [24]. The specimen was oxidised in the air for 22h. The thermogravimetric oxidation results show that oxidation kinetics followed the parabolic law. According to the XRD results, the outer scale has $Fe_2O_3$ while the inner scale is $NiFe_2O_4$ phase. The oxidation rate constant was $9.568 \cdot 10^{-4}$ $kg^2m^{-4}h^{-1}$. A short-term electrolysis test was performed for 30 min on pre-oxidised and non-oxidized anodes and it observed that in the case of the pre-oxidised anode, small bubbles were seen on the surface while on the surface of the non-oxidised, no bubbles were evolved. It was concluded that the anode with pre-oxidation has better corrosion resistance.

### 3.2. Fe–Ni–Al alloy

Guan et al. [25] investigated the corrosion and oxidation behaviour of Fe–Ni–Al anode in $NaF–AlF_3–NaCl–CaF_2–Al_2O_3$ at 850 °C. When the anode is immersed into the electrolyte, the oxide layer is formed initially due to the high-temperature oxidation. When the anode is electrified, the aluminium-oxygen-fluoride complex ion $[Al_2O_2F_4]^{2-}$ in the molten salt migrates to the oxide surface on the anode leading to the loss of electrons of oxygen anion $O^{2-}$, tends to become an adsorbed oxygen atoms. The $AlF_4^-$ complex ion is released and dissociates into $AlF_3$ and $F^-$. The oxygen atoms formed can then oxidize metal on the anode surface or combine into $O_2$. $F^-$ ion can

migrate to the oxide layer and expand to the interface of molten salts, leads to the formation of $AlF_3$ in the oxide film with $Al^{3+}$ ions. A large amount of $AlF_3$ phase in the inner and outer oxide layers on the cross-section of the anode. Atoms and ions such as $Al^{3+}/Fe^{3+}$ in the anode oxide scale migrate outward to form $Fe_2O_3$ or $FeAl_2O_4$ film at the interface of molten salt.

The investigation shows that the corrosion layer contains two sublayers and includes $Fe_2O_3$, $Fe_3O_4$, $Al_2O_3$, NiO, $NiFe_2O_4$, and $FeAl_2O_4$. The fluorine salt has a corrosive effect on the oxide film. Al inclusion in the alloy has more impact than Fe and Ni, where it is preferentially oxidized and serves as a connection between the oxide scale and the metal to have better adhesion on the former. The $FeNi_2O_4$ phase has a major impact and significantly contributes to the alloys corrosion resistance. Addition of small amounts of Al to the alloy improves the corrosion resistance, and alloy with the composition 57.9Fe–38.2Ni–3.9Al possesses better corrosion resistance against the fluoride melts.

### 3.3. Cu–Ni–Fe alloy

Importance of Cu proportion in the Cu–Ni–Fe alloy, which is used as an anode in aluminium electrolysis is examined in [26]. Initially, the samples were made of three different wt.% composition with Cu (45, 55 and 65 wt.%) and Ni/Fe weight ratio is 1.33. The oxidation behaviour of the samples was tested in $KF–AlF_3$ melt (45 wt.% KF + 50 wt.% $AlF_3$+ 5 wt.% $Al_2O_3$) at 700 °C. The electrolysis test was conducted for 20h with anode current density of 0.5 $A/cm^2$. The cell voltage increased after 10 h of electrolysis resembling the decrease in the electrical conductivity. The oxidation scale constitutes of three main phases: CuO, $Cu_2O$ and $NiFe_2O_4$. The CuO layer is initially formed on the anode surface while the nickel spinal ($NiFe_2O_4$) starts to grow underneath the outer layer (CuO). The CuO scale acts as a sacrificial layer. The CuO layer in contact with melt is readily dissolved and enough Cu content should be present in the alloy to counter the dissolution. This gives the required time for the $NiFe_2O_4$ to completely from. $NiFe_2O_4$ scale also stops the melt to come in contact with the alloy, keeping it safe from getting dissolved. The study concludes that the high content of Cu is recommended in the alloy. It is also worth noting that the passivation behaviour of the Cu–65 anode was improved with the addition of 1.4 wt.% of O [27]. The results from the electrolysis tests conducted on 65Cu–20Ni–15Fe anode in potassium melts show that the anode wear rate was 1.8 cm/year with the purity of produced aluminium being 99.4% [28]. An electrolysis test with cell 300 A was performed using Cu-65 anode and titanium diboride cathode in eutectic potassium and sodium cryolites at 700 and 950 °C respectively. It was noticed that the corrosion rate constant in potassium cryolite at 700 °C was $10^4$ less than in sodium cryolites at 950 °C [29]. Cold spray technique can be used to spray the Cu65–Ni20–Fe15 particle on the substrate which eases the fabrication of large surface area anode [30–32].

The oxidation behaviour and corrosion performance of 52Cu–30Ni–18Fe alloy with and without the addition of La in KF–NaF–$AlF_3$ melt at low-temperature were studied in [33]. The findings stated that the oxidation kinetics of $(52Cu–30Ni–18Fe)_{1–x}La_x$ ($x$ =0, 0.5, 1, 2wt.%) alloy under 1 atm oxygen atmosphere at 850°C follow the parabolic law. The outer oxide scale comprises of CuO while the inner oxide scale contains NiO, $Fe_2O_3$ or nickel spinal ($NiFe_2O_4$). With the addition of La to the 52Cu–30Ni–18Fe alloy, the oxidation mechanism has simultaneous processes where the inner diffusion of O attributes to the formation of nickel spinel while the outwards diffusion of Cu leads to the formation of CuO (which acts as a sacrificial layer). 0.5 wt.% addition of La to the 52Cu–30Ni–18Fe alloy reduced the corrosion rate from 1.9 to 1.8 cm/year.

An electrolysis test was conducted using 20Cu–42Ni–38Fe anode and $TiB_2$ cathode in a vertical electrode cell with the KF–NaF–$AlF_3$ melt (CR of 1.3 and NaF/(NaF + KF) molar ratio of 0.2) at 800 °C and is reported in [34]. The electrolysis was carried out on the pre-oxidised and non-oxidised anodes at 0.5 A/cm$^2$ and 1 A/cm$^2$ current densities. The produced aluminium purity and the current efficiency were estimated. The results show the pre-oxidation of the anode in this particular case has neither significant impact on the current efficiency nor the produced aluminium purity. Table 2 summarizes the results of the work.

He Han-Bing et al. [35] added 1 wt.% of BaO to increase the corrosion resistance of Cu–NiO–$NiFe_2O_4$ anodes in $Na_3AlF_6$–$AlF_3$–$CaF_2$–$Al_2O_3$ bath. On the one hand, BaO can effectively promote relative density of $x$Cu/(10NiO–$NiFe_2O_4$) cermet and thus improve its corrosion resistance; on the other hand, BaO in the grain boundary maybe accelerate the corrosion of cermet. The corrosion rates were in the range of 2.15–8.30 cm/year.

**Table 2**.

Experimental parameters and the current efficiency, purities achieved in different experiments [34]

| Anode (20Cu–42Ni–38Fe) | Current density (A/cm$^2$) | Cell voltage (V) | Current efficiency | Aluminium purity |
|---|---|---|---|---|
| Pre-oxidised | 0.5 | 3.5–3.7 | 72 | 99.78 |
| Pre-oxidised | 1.0 | 4.8–5.2 | 73 | 99.75 |
| Non-oxidised | 1.0 | 4.75–5.75 | 71 | 99.71 |

Electrolysis tests in the low-temperature slurry-fluoride NaF-$AlF_3$ melt were performed by Gallino et al. [36] at 0.75 A/cm$^2$ with Cu–Ni–Fe anode. It was proved that homogenization

significantly improves the anode performance. The cell voltage and the resistance were stable during the operation of the pre-heat treated anode material, whereas catastrophic corrosion was observed on as-cast material at much shorter times. The cell was operated for 500 hours with average current efficiency for the entire run above 95%. The Cu, Fe and Ni content in the produced Al was less than 0.1 wt.%. Another homogenization treatment study was performed by Jucken et al. [37–38]. It was shown that the post-casting homogenization treatment of 65Cu–20Ni–15Fe does not lead to any significant decrease in the aluminium and electrolyte contamination levels despite its ability to form a more coherent inner $NiFe_2O_4$ layer than the as-cast alloy. It does not prevent the formation of $FeF_3$ and $NiF_2$ at the alloy/oxide interface. It also suggests that an appropriate pre-oxidation of the homogenized 65Cu–20Ni–15Fe alloy prior using may improve its corrosion resistance in cryolite media.

### 3.4. Ni–Fe alloy

Anodic behaviour of Ni–Fe alloy in the cryolite-alumina melt at 960 °C was investigated in [39]. Before the electrolysis, the anode was oxidised at 800 °C for 48 h and protective layers were formed with $Fe_2O_3$, $Ni_xFe_{3-x}O_4$ and $Ni_xFe_{1-x}O$ phases. Anodes with Ni content of 50–65 wt.% performed well during short-term electrolysis, with a steady potential of 3–3.5V vs. $AlF_3$/Al.

The oxide layer growth is indulged by the reactions, such as metal dissolution, oxygen evolution, and fluoridation which happen simultaneously. The reaction scales possessed non-homogeneity, excessive porosity, and poor surface adherence. The studies show that the only nickel ferrite offers adequate stability, adhesion and imperviousness towards cryolite melt. Another alternative was to cover the anode with a layer of electrodeposited metal, which leads to a decrease in the diffusion of Fe to the anode surface. In conclusion, pre-oxidized anodes performed better than the anodes without prior oxidation.

Co was added to the Ni–Fe alloy and the corrosion behaviour of the ternary alloy $Ni_xFe_yCo_z$ alloys (where $x/y$(wt). = 1 and 1.85; $z$ = 0, 10, 30 and 50 wt.%) was studied at 800 °C under air atmosphere [40]. In the high Co content alloy, multi-layer Co-rich scales containing $Ni_xCo_{3-x}O_4$, $Co_xFe_{3-x}O_4$, $Co_3O_4$ and CoO phases are formed. In alloys having lower cobalt content, iron-rich scales are produced with the major phases being $Ni_xFe_{3-x}O_4$, $Ni_xFe_{1-x}O$ and $Co_xFe_{3-x}O_4$, $Fe_2O_3$. The oxidation resistance of the alloy increases when the Co content (10% and 30%) is added to Ni–Fe (weight ratio = 1).

### 3.5. Cu – Al alloy

Electrochemical behaviour of Cu–Al based alloys with compositions 86Cu–9Al–5Fe, 90Cu–10Al and 88.3Cu–10Al–1.7Be was tested in KF – $AlF_3$ – $Al_2O_3$ melts and suspensions [41–43]. The

influence of alumina volume fraction and the composition of anode were characterised by stationary and non-stationary polarization. The findings show that with an increase in the volume fraction of alumina in the melt leads to a considerable decrease in apparent limiting current density of the oxygen evolution and the metal oxidation for the anode compositions. It also leads to the drastic increase in the resistance due to several reasons: accumulation of anode oxidation products and bubbles in the anode layer, active surface area decrease, growth of oxide layer and structural changes of the oxide layer. The $CuAlO_2$ and $Cu_2O$ compounds were found to be the most abundant compounds in all oxide layers. The 90Cu–10Al anode, the aluminium oxide suspension based on the KF–$AlF_3$–$Al_2O_3$ system with a volume fraction no more than 0.09 (with 5% $Al_2O_3$) at a temperature of at least 750 °C are recommended for further studies. The electrolysis test was performed by using 90Cu–10Al anode and tungsten cathode at 800 °C in KF–$AlF_3$–$Al_2O_3$ (cryolite ratio = 1.4) for 18 hours [15]. The current efficiency of 84.4% was attained with a produced aluminium purity of 99.4%.

Hryn et al. [44] reported the successful 1000 A test performed in the 1.3KF–$AlF_3$–$Al_2O_3$ melt with aluminium bronze anode at 750 °C. The current density was as high as 0.5 A/cm$^2$ and the interelectrode distance was 2.2 cm. The duration was 24 hours. The produced metal contained 2.8 wt.% of Cu due to the exposure of the anode to the electrolyte without polarization for 30 minutes before the test. The purity improved in later published work. Khramov et al. [16] studied the anodic behaviour of the 82Cu–8Al–5Ni–5Fe alloy in KF–$AlF_3$–$Al_2O_3$ electrolyte. The anode performed well and could be applied in larger-scale experiments.

## 4. Alternative inert anodes

Liu et al. [45] proposed oxygen pumping anode (OPA) for the electrowinning of aluminium. This anode is a closed-end tube made of zirconium-oxide based ceramic (YSZ) stabilized by the addition of yttrium oxide filled with $LaMnO_3$ with nickel wires used as current leads. This anode route exhibited more stability than the established inert anode for aluminium electrolysis, due to the "induced" thermodynamic stability driven by the chemical and electrochemical potential advantage and the surface separation of $O^{2-}$ diffusion and $O_2$ evolution.

Xiao et al. [46] studied the effect of hydrogen on the 96$SnO_2$–2CuO–2$Sb_2O_3$ anode potential during the electrolysis at 0.1–0.2 A/cm$^2$ in NaF–$AlF_3$ at 850 °C. The decrease of anode potential reached 0.8–1.0 V. Constantin [47] studied similar $SnO_2$-based ceramic anode in the NaF–$AlF_3$–$CaF_2$–$Al_2O_3$ melt. The current efficiency values around 91.5 % were achieved at 940–960 °C, 0.7–0.8 A/cm$^2$ and 2–3 cm of interelectrode distance.

Cermets still get considerable attention in the recent publications. Tian et al. [48] found that The corrosion rate of 17Ni/(90$NiFe_2O_4$−10NiO) cermet during electrolysis can be reduced by an

increase in the oxygen content of the sintering atmosphere. The corrosion rate of anode prepared in the atmosphere with the oxygen content of $2 \cdot 10^{-3}$ wt. % is 2.71 cm/year. For the anode prepared in the vacuum, its corrosion rate is 6.46 cm/year. The reason is that the decrease of the oxygen content in the sintering atmosphere will cause the increase of the content of Fe(II) in $NiFe_{2x}O_{4-y-z}$, which may dissolve more easily than that of Fe(III). The content of NiO also increases. Yang et al. [49] studied the corrosion process of (Cu–Ni–Fe)/(90$NiFe_2O_4$–10NiO) cermet anode. A 200 A long-term (1000 hours) aluminium electrolysis test showed that the corrosion rate of the cermet anode was less than 0.99 cm/year, which satisfied the aluminium industrial demands.

Wang et al. [50] studied the effect of $TiO_2$ addition on grain growth, the corrosion behaviour of $NiFe_2O_4$-based cermet anode, the bubble evolution and the anodic overvoltage in the NaF – $AlF_3$ – $CaF_2$ – $Al_2O_3$ melts at 980 °C. The kinetic index of grain growth decreased with increasing temperature. The $TiO_2$ addition inhibited grain growth for $NiTiO_3$ and $Fe_2TiO_5$. The average activation energy of grain growth for 1.0 wt.% $TiO_2$-doped $NiFe_2O_4$ ceramic samples with a sintering range from 1373 to 1673 K dropped from 675.30 to 183.47 kJ/mol. The bubbles diameter before releasing was reduced with increasing the current density. After adding a small amount of $TiO_2$, a minor reduction in anodic overvoltage of $NiFe_2O_4$-based anodes can be obtained.

Wu et al. [51] proposed the procedure to make $NiFe_2O_4$-based nano-cermet and achieved 100 °C lower sintering temperature and high-temperature semiconductor properties. The preparation procedure involved homogeneous precipitation, moulding and normal pressure sintering. The corrosion rate in the "commercial" electrolyte was less than 3 cm/year.

Liu et al. [52] studied cermet anodes where $NiFe_2O_4$ spinel was synthesized by solid-state reaction of NiO and $Fe_2O_3$ powders at 950 °C. The ceramic phase formed a mesh structure in the composite anode materials with $NiFe_2O_4$ content higher than 50 wt.%. The substitution reaction between Fe in the alloy phase and Ni in the oxide phase occurred during sintering under an $N_2$ atmosphere. The (52Cu–30Ni–18Fe)–$x$$NiFe_2O_4$ cermet showed excellent corrosion resistance in the low-temperature KF – NaF – $AlF_3$ melt during electrolysis. The scale was stated to have a self-repairing function because of the synergistic reaction between the alloy phase with added Fe and the oxide phase. The estimated wear rate of the (52Cu–30Ni–18Fe) – $x$$NiFe_2O_4$ anodes with $x$ = 40 wt.%, 50 wt.%, 60 wt.%, and 70 wt.% were 2.19, 2.02, 1.89, and 1.76 cm/year, respectively.

A new type of Fe–Ni ceramet inert anode with the NiO contents of 0, 10, 20 and 30 wt.%, which played an important role in hindering the oxidation process, was proposed by Yang et al. [53]. The preexisting oxide phase shortened the time for the formation of the oxide scale on the sample, which promoted the formation of continuous dense scale with the good adhesion to substrate materials during high-temperature oxidation. The appearance of NiO at the grain boundary hindered the oxidation of the metal phase. $Co_xNi_{1-x}O$ materials have been prepared and

characterized by Mohammadkhani et al. [54]. (Co, Ni)O solid solutions contaminated by WC were firstly produced by prolonged mechanical milling (20 hours). WC contamination was eliminated by decreasing the ball milling time from 20 hours to 12 minutes and using a high-temperature heat-treatment step (10 hours at 1000 °C). At 1000 °C, $Co_xNi_{1-x}O$ solid solutions are stable over the whole composition range. In contrast, at 700 and 800 °C, $Co_xNi_{1-x}O$ are only stable for $x \leq 0.22$ and $x \leq 0.46$, respectively. The use of single-phase (Co, Ni)O powders as raw materials for the preparation by thermal spraying of protective coating on metallic inert anodes is in progress and their anodic behaviour for Al electrolysis will be presented in the future.

Pasquet et al. [55] reported the manufacturing of the coherent but porous 3D cermet inert anode based on spinel ferrites and metallic copper for the first time. This study revealed an original microstructure of the cermet parts regardless of the manufacturing parameters. The SLM process allowed to create a nanostructured material from a micrometric powders mixture while maintaining a spinel oxide and a metal as main phases. The phase compositions were slightly different from those of the initial powders. Microstructure and changes in phase composition were explained with the local melting of the compounds involved by the high temperatures reached under a focused laser beam. First galvanostatic electrolysis under industrial conditions with cryolitic medium ($Na_3AlF_6$) was performed at 980 °C and 0.6 A/cm$^2$ for 4 hours with an electrode of 5 mm in diameter. The diameter of the electrode ranged from 2 to 5 mm after the test. The improvement of the corrosion resistance is the subject of further work.

## 5. Recent industrial attempts

RUSAL has implemented several strategies to minimise pollution and energy consumption during the electrolysis process. Global environmental standards have already been implemented on the existing smelters and no. of pre-baked potlines has been increased. Few of the achievements of the RUSAL in the recent past are as below [56]:

– Testing area for inert anode cells has already been established that are intended to replace Vertical Stud Soderberg (VSS) cells;

– Introduction of new Eco-Søderberg cells containing environmental indicators that are comparable to pre-baked cells;

– Use of cutting-edge online and video systems for cell condition and emissions control monitoring;

– High-performance GTCs construction;

– Development and execution of technologies for sulfur recovery;

– Solid waste management, SPL recycling.

Continuous attempts are carried out to come up with an inert anode which can retrofit in the presently used cell.

Several publications discussed the ELYSIS technology [57] for aluminium production with vertical inert anodes and wettable cathodes. It was jointly announced by ALCOA, RTA and Apple to be commercialized in 2024. It has claimed to extend anode life by around 30 times (about 2.5 years) as compared to carbon anode and reduce the operating cost by 15% and increase productivity.

## 6. Factors influencing the performance of the anode

Certain important factors can be identified which influence the performance of the anode in the melts.

– Electrolysis temperature, a low operating temperature can reduce the corrosion rate of the anode [58];

– Pre-oxidation of the anode can improve the electrochemical behaviour of the anode, as the pre-oxidized anodes possess a thick scale which can readily protect the anode from the dissolution;

– Using the suspension can reduce the contamination of the produced aluminium from the anode products [59];

– The bubble size on the anode surface determines the mass transfer coefficient. The mass transfer on the anode surfaces tends to be lower when the bubble size is small;

– The low solubility of the oxide scales in the melts can reduce the corrosion rate of the anode;

– The cell design optimization, in which the electrodes are vertical and have wettable cathode.

## 7. The bigger picture on cleaner aluminium production

It is a well-established fact that almost a value between 12 and 17 metric tonnes of $CO_2$ equivalents per tonne of aluminium. Although two-third of the emission is caused by the electricity used in the electrolysis process is generated from fossil fuels such as coal, natural gas and oil. The carbon-free aluminium production is not solely dependent on inert anodes development but the emission can be reduced by using cleaner forms of energy (hydroelectric powerplant). The greenhouse gases emission can be controlled to a certain level by implementing the following steps [60–61]:

– Aluminium production should be carried out in countries where the energy generation is through the low emission source;

– The cells older than 50 years should be replaced with new ones which have low energy consumption and can monitor/control the anode effect, so a considerable amount of PFC emission can be reduced;

– High-quality anode usage with better anode cover can reduce the net prebaked carbon anode consumption;

– Electrolytes should be well saturated with alumina particularly before and during the anode charge, which can reduce the non-anode effect PFC emissions.

$CO_2$ evolved can be successfully captured and electrochemically converted to carbon and oxygen using Li–Na–K carbonates, a Ni cathode and a $SnO_2$ inert anode at 500 °C as proposed by Yin et al. [62].

## 8. Summary

In the past decade, a lot of development has been made in developing metallic inert anodes. The researchers have given much attention to binary or trinary alloys with Cu being a common element in most of the alloys. Some researchers have stated that pre-oxidizing the anode materials can improve the corrosion resistance. The use of low-temperature electrolytes can improve the stability of the anode oxide scale. The clean energy source is recommended to reduce greenhouse gas emission. Considerable steps should be taken to reduce the cell energy consumption. No industry has successfully launched an inert anode for the aluminium electrolysis yet. Future will show whether the inert anodes can ever replace the consumable carbon anode used for aluminium reduction.

## Acknowledgements

***The work is performed as a part of the state assignment for the science of Siberian Federal University, project number FSRZ-2020-0013.***

***Use of equipment of Krasnoyarsk Regional Center of Research Equipment of Federal Research Center "Krasnoyarsk Science Center SB RAS" is acknowledged.***

## References

1. Kvande H., Haupin W. Inert Anodes for Al Smelters: Energy Balances and Environmental Impact. *JOM*. 2001. Vol. 53, Iss. 5. pp. 29–33.

2. Haraldsson J., Johansson M. T. Review of Measures for Improved Energy Efficiency in Production-Related Processes in the Aluminium Industry – from Electrolysis to Recycling. *Renewable and Sustainable Energy Reviews*. 2018. Vol. 93. pp. 525–548.

3. Solheim A. Inert Anodes — the Blind Alley to Environmental Friendliness? *Minerals, Metals and Materials Series: Light metals.* 2018. pp. 1253–1260.

4. Padamata S. K., Yasinskiy A. S, Polyakov P. V. Progress of Inert Anodes in Aluminium Industry: Review. *Journal of Siberian Federal University: Chemistry*. 2018. Vol. 11, Iss. 1. pp. 18–30.

5. Pawlek R. P. Inert Anodes for the Primary Aluminium Industry: an Update. *TMS Light Metals*. 1996. pp. 243–248.

6. Pawlek R. P. Inert Anodes: an Update. *TMS Light Metals*. 2002. pp. 449–456.

7. Pawlek R. P. Inert Anodes: an Update. *TMS Light Metals*. 2004. pp. 283–287.

8. Pawlek R. P. Inert Anodes: an Update. *TMS Light Metals*. 2008. pp. 1039–1045.

9. Pawlek R. P. Inert Anodes: an Update. *TMS Light Metals*. 2014. pp. 1309–1313.

10. Galasiu I., Galasiu R., Thonstad J. Inert Anodes for Aluminium Electrolysis. Düsseldorf: Aluminium-Verlag, 2007. 212 p.

11. Glucina M., Hyland M. Laboratory-Scale Performance of a Binary Cu–Al Alloy as an Anode for Aluminium Electrowinning. *Corrosion Science*. 2006. Vol. 48, Iss. 4. pp. 2457–2469.

12. Keller R., Rolseth S., Thonstad J. Mass Transport Considerations for the Development of Oxygen-Evolving Anodes in Aluminum Electrolysis. *Electrochimica Acta*. 1997. Vol. 42, Iss. 12. pp. 1809–1817.

13. Antipov E. V., Borzenko A. G., Denisov V. M., Filatov A. Yu., Ivanov V. V., Kazakov S. M., Mazin P. M., Mazin V. M., Shtanov V. I., Simakov D. A., Tsirlina G. A., Vassiliev S. Yu., Velikodny Yu. A. Electrochemical Behavior of Metals and Binary Alloys in Cryolite-Alumina Melts. *TMS Light Metals*. 2006. pp. 403–408.

14. Oudot M., Cassayre L., Chamelot P., Gibilaro M., Massot L., Pijolat M., Bouvet S. Layer Growth Mechanisms on Metallic Electrodes Under Anodic Polarization in Cryolite-Alumina Melt. *Corrosion Science*. 2014. Vol 79. pp. 159–168.

15. Padamata S. K., Yasinskiy A. S., Polyakov P. V. Electrode Processes in KF–$AlF_3$–$Al_2O_3$ Melts. *New Journal of Chemistry*. 2020. Vol. 44, Iss. 13. pp. 5152–5164.

16. Khramov A. P., Kovrov V. A., Zaikov Yu. P, Chumarev V. M. Anodic Behaviour of the $Cu_{82}Al_8Ni_5Fe_5$ Alloy in Low-Temperature Aluminium Electrolysis. *Corrosion Science*. 2013. Vol 70. pp. 194–202.

17. Suzdaltsev A., Khramov A., Kovrov V., Limanovskaya O., Nekrasov V., Zaikov Y. Voltammetric and chronopotentiometric study of nonstationary processes at the oxygen-evolving anodes in KF–NaF–$AlF_3$–$Al_2O_3$ melt. *Materials Science Forum*. 2016. Vol. 884. pp. 19–26.

18. Tang D., Zheng K., Yin H., Mao X., Sadoway D. R., Wang D. Electrochemical Growth of a Corrosion-Resistant Multi-Layer Scale to Enable an Oxygen-Evolution Inert Anode in Molten Carbonate. *Electrochimica Acta.* 2018. Vol. 279. pp. 250–257.

19. Ndong G. K., Xue J., Feng L., Zhu J. Effect of Anodic Polarization on Layer-Growth of Fe–Ni–Cr Anodes in Cryolite-Alumina Melts. *TMS 6th International Symposium on High-Temperature Metallurgical Processing.* 2015. pp. 83–90.

20. Meyer P., Massot L., Gibilaro M., Bouvet S., Laurent V., Marmottant A., Chamelot P. Electrochemical Degradation Mechanism of a Cermet Anode for Aluminum Production. *Materials Sciences and Applications*. 2019, Vol. 10. pp. 614–629

21. Meyer P., Gibilaro M., Massot L., Pasquet I., Tailhades P., Bouvet S., Chamelot P. Comparative Study on the Chemical Stability of $Fe_3O_4$ and $NiFe_2O_4$ in Molten Salts. *Materials Science and Engineering: B.* 2019. Vol. 228. pp. 117–122.

22. Cao D., Shi Z., Shi D., Xu J., Hu X., Wang Z. Electrochemical Oxidation of Fe–Ni Alloys in Cryolite–Alumina Molten Salts at High Temperature. *Journal of the Electrochemical Society*. 2019. Vol. 166, Iss. 4. pp. E87–E96.

23. Cao D., Ma J., Shi Z., Shi D., Xu J., Hu X., and Wang Z. Corrosion Behavior of Fe–Ni Alloys in Molten $KF–AlF_3–Al_2O_3$ Salts at 700 °C. *Corrosion Science.* 2019. Vol. 156. pp. 32–43.

24. Huang Y., Yang Y., Zhu L., Liu F., Wang Z., Gao B., Shi Z., Hu X. Electrochemical Behavior of Fe-Ni Alloys as an Inert Anode for Aluminum Electrolysis. *International Journal of Electrochemical Science*. 2019. Vol. 14. pp. 6325–6336.

25. Guan P., Aimin Liu A., Shi Z., Hu X., Wang Z. Corrosion Behavior of Fe-Ni-Al Alloy Inert Anode in Cryolite Melts. *Metals.* 2019. Vol. 9, Iss 4. DOI: 10.3390/met9040399.

26. Gavrilova E., Goupil G., Davis B., Guay D., Roué L. On the Key Role of Cu on the Oxidation Behavior of Cu–Ni–Fe Based Anodes for Al Electrolysis. *Corrosion Science*. 2015. Vol. 101. pp. 105–113.

27. Goupil G., Helle S., Davis B., Guay D., Roué L. Anodic Behavior of Mechanically Alloyed Cu–Ni–Fe And Cu–Ni–Fe–O Electrodes for Aluminum Electrolysis in Low-Temperature $KF–AlF_3$ Electrolyte. *Electrochimica Acta.* 2013. Vol. 112. pp. 176–182.

28. Goupil G., Bonnefont G., Idrissi H., Guay D., Roué L. Consolidation of Mechanically Alloyed Cu–Ni–Fe Material by Spark Plasma Sintering and Evaluation as Inert Anode for Aluminum Electrolysis. *Journal of alloys and compounds*. 2013. Vol. 580. pp. 256–261.

29. Beck T. R., Macrae C. M., Wilson N. C. Metal Anode Performance in Low-Temperature Electrolytes for Aluminum Production. *Metallurgical And Materials Transactions B*. 2011. Vol. 42, Iss. 4. pp. 807–813.

30. Goupil G., Helle S., Irissou E., Poirier D., Legoux J. G., Guay D., Roué L. Cold Spray Deposition of Mechanically Alloyed Cu–Ni–Fe Material for Application as Inert Anodes for Aluminum Production. *Light Metals*. 2013. pp. 1283–1287.

31. Goupil G., Jucken S., Poirier D., Legoux J. G., Irissou E., Davis B., Guay D., Roue L. Cold Sprayed Cu–Ni–Fe Anode for Al Production. *Corrosion Science.* 2015. Vol. 90. pp. 259–265.

32. Jucken S., Martin M.H., Irissou E., Davis B., Guay D., and Roue L. Cold-Sprayed Cu–Ni–Fe Anodes for $CO_2$-free Aluminum Production. *Journal of Thermal Spray Technology*. 2020. Vol. 29, Iss. 4. pp. 670–683.

33. Ying L., Yong Z., Wei W., Dongsheng L., Junyi M., Juan D. The Effect of La on the Oxidation and Corrosion Resistance of Cu52Ni30Fe18 Alloy Inert Anode for Aluminum Electrolysis. *Arabian Journal for Science and Engineering*. 2018. Vol. 43, Iss. 11. pp. 6285–6295.

34. Gunnarsson G, Óskarsdóttir G., Frostason S., Magnússon J. H. Aluminum Electrolysis with Multiple Vertical Non-Consumable Electrodes in a Low Temperature Electrolyte. *Minerals, Metals and Materials Series: Light metals.* 2019. pp. 803–810.

35. He H.-B., Xiao H.-N., Zhou K.-Ch. Effect of Additive BaO on Corrosion Resistance of xCu/(10NiO-$NiFe_2O_4$) Cermet Inert anodes for aluminum electrolysis. *Transactions of Nonferrous Metals Society of China*. 2011. Vol. 21. pp. 102–108.

36. Gallino I., Kassner M. E., Busch R. Oxidation and Corrosion of Highly alloyed Cu–Fe–Ni as Inert Anode Material for Aluminum Electrowinning in as-Cast and Homogenized Conditions. *Corrosion Science*. 2012. Vol. 63. pp. 293–303.

37. Jucken S., Tougas B., Davis B., Guay D., Roué L. Study of Cu–Ni–Fe Alloys as Inert Anodes for Al Production in Low-Temperature KF–$AlF_3$ Electrolyte. *Metallurgical And Materials Transactions B*. 2019. Vol. 50, Iss. 6. pp. 3103–3111.

38. Jucken S., Schaal E., Tougas B., Davis B., Guay D., Roue L. Impact of a Post-Casting Homogenization Treatment on the High-Temperature Oxidation Resistance of a Cu–Ni–Fe alloy *Corrosion Science*. 2019. Vol. 147. pp. 321–329.

39. Chapman V., Welch B. J., Skyllas-Kazacos M. Anodic Behaviour of Oxidised Ni–Fe Alloys in Cryolite–Alumina Melts. *Electrochimica Acta*. 2011. Vol. 56, Iss. 3. pp. 1227–1238.

40. Chapman V., Welch B. J., Skyllas-Kazacos M. High Temperature Oxidation Behaviour of Ni–Fe–Co Anodes for Aluminium Electrolysis. *Corrosion Science*. 2011. Vol. 53, Iss. 9. pp. 2815–2825.

41. Yasinskiy A. S., Padamata S. K., Polyakov P. V., Samoilo A. S., Suzdaltsev A. V., Nikolaev A. Y. Electrochemical Behaviour of Cu-Al Oxygen-Evolving Anodes in Low-Temperature Fluoride Melts and Suspensions. *Minerals, Metals and Materials Series: Light metals.* 2020. pp. 591–599.

42. Padamata S. K., Yasinskiy A. S., Polyakov P. V. Anodic Process on Cu-Al Alloy in KF–$AlF_3$–$Al_2O_3$ Melts and Suspensions. *Transactions of Nonferrous Metals Society of China*. 2020. (In press)
43. Yasinskiy A. S., Padamata S. K., Polyakov P. V., Vinogradov O. O. Anodic process on aluminium bronze in low-temperature cryolite-alumina melts and suspensions. *Tsvetnye Metally*. 2019. No. 9. pp. 42–49. DOI: 10.17580/tsm.2019.09.07
44. Hryn J., Tkacheva O., Spangenberger J. Initial 1000A Aluminum Electrolysis Testing in Potassium Cryolite-Based Electrolyte. *TMS Light Metals*. 2013. pp. 1289–1294.
45. Liu C., Ji X., Zhang P., Chena Q., Banks C. E. An Oxygen Pumping Anode for Electrowinning Aluminium. *Physical Chemistry Chemical Physics*. 2013. Vol. 15, Iss. 17. pp. 6350–6354.
46. Xiao S., Mokkelbost T., Paulsen O., Ratvik A. P., Haarberg G. M. $SnO_2$-Based Gas (Hydrogen) Anodes for Aluminum Electrolysis. *Transactions of Nonferrous Metals Society of China*. 2014. Vol. 24, Iss. 12. pp. 3917–3921.
47. Constantin V. Influence of the Operating Parameters Over the Current Efficiency and Corrosion Rate in the Hall–Heroult Aluminum Cell With Tin Oxide Anode Substrate Material. *Chinese Journal of Chemical Engineering.* 2015. Vol. 23, Iss. 4. pp. 722–726.
48. Tian Z., Guo W., Lai Y., Zhang K., Li J. Effect of Sintering Atmosphere on Corrosion Resistance of Ni/($NiFe_2O_4$−10NiO) Cermet Inert Anode for Aluminum Electrolysis. *Transactions of Nonferrous Metals Society of China*. 2016. Vol. 26, Iss. 11. pp. 2925–2929.
49. Yang W.-J., Guo J., Li J., Zhang G., He L.-Q., Zhou K.-Ch. A Self-Repairing Cermet Anode: Preparation and Corrosion Behavior of (Cu–Ni–Fe)/$NiFe_2O_4$ Cermet with Synergistic Action. *Journal of the American Ceramic Society.* 2016. Vol. 100, Iss. 3. pp. 887–893.
50. Wang B., Du J., Liu Y., Fang Z., Hu P. Effect of $TiO_2$ Addition on Grain Growth, Anodic Bubble Evolution and Anodic Overvoltage of $NiFe_2O_4$-Based Composite Inert Anodes. *Journal of Materials Engineering and Performance*. 2017. Vol. 26, Iss. 11. pp. 5610–5619.
51. Wu X., Zhu W., Luo K., Wu S. Production of $NiFe_2O_4$ Nanocermet for Aluminium Inert Anode. *TMS Light Metals*. 2017. pp. 1357–1364.
52. Liu Y., Zhang Y., Wang W., Li D., Ma J. Microstructure and Electrolysis Behavior of Self-Healing Cu–Ni–Fe Composite Inert Anodes for Aluminum Electrowinning. *International Journal of Minerals, Metallurgy and Materials.* 2018. Vol. 25, Iss. 10. pp. 1208–1216.
53. Yang W.-J., Wang Y., Zhai H.-F., Fan J. Effect of NiO Addition on the High-Temperature Oxidation and Corrosion Behaviors of Fe–Ni Alloy as Inert Anode Material for Aluminum Electrolysis. *Journal of Materials Science*. 2020, Vol. 55, Iss. 9. pp. 4065–4072.
54. Mohammadkhani S., Schaal E., Dolatabadi A., Moreau C., Davis B., Guay D., Roué L. Synthesis and Thermal Stability of (Co,Ni)O Solid Solutions. *Journal of the American Ceramic Society*. 2019. Vol. 102, Iss. 9. pp. 5063–5070.

55. Pasquet I., Baco-Carles V., Chamelot P., Gibilaro M., Massot L., Tailhades Ph. A Multimaterial Based on Metallic Copper and Spinel Oxide Made by Powder Bed Laser Fusion: a New Nanostructured Material for Inert Anode Dedicated to Aluminum Electrolysis. *Journal of Materials Processing Technology*. 2020. Vol. 278. 116452. DOI: 10.1016/j.jmatprotec.2019.116452

56. Mann V., Buzunov V., Pingin V., Zherdev A., Grigoriev V. Environmental Aspects of UC RUSAL's Aluminum Smelters Sustainable Development. *Minerals, Metals and Materials Series: Light metals.* 2019. pp. 553–563.

57. Gupta A., Basu B. Sustainable Primary Aluminium Production: Technology Status and Future Opportunities. *Transactions of the Indian Institute of Metals.* 2019. Vol. 72, Iss. 8. pp. 2135–2150.

58. Padamata S. K., Yasinskiy A. S., Polyakov P. V. Electrolytes and its Additives Used in Aluminium Reduction Cell: a Review. *Metallurgical Research & Technology*. 2019. Vol. 116, Iss. 4. 410. DOI: 10.1051/metal/2018136

59. Yasinskiy A., Suzdaltsev A., Padamata S. K., Polyakov P., Zaikov Y. Electrolysis of Low-Temperature Suspensions: an Update. *Light metals.* 2020. pp. 626–636.

60. Saevarsdottir G., Kvande H., Welch B. J. Reducing the Carbon Footprint: Aluminium Smelting with Changing Energy Systems and the Risk of Carbon Leakage. *Light metals.* 2020. pp. 726–734.

61. Saevarsdottir G., Kvande H., Welch B. J. Aluminum Production in the Times of Climate Change: The Global Challenge to Reduce the Carbon Footprint and Prevent Carbon Leakage. *JOM*. 2020. Vol. 72, Iss. 1. pp. 296–308.

62. Yin H., Mao X., Tang D., Xiao W., Xing L., Zhu H., Wang D., Sadoway D. R. Capture and Electrochemical Conversion of $CO_2$ to Value-Added Carbon and Oxygen by Molten Salt Electrolysis. *Energy & Environmental Science*. 2013. Vol. 6, Iss. 5. pp. 1538–1545.